

Modeling long term Enhanced in situ Biotenitrification and induced heterogeneity in column experiments under different feeding strategies

Rodríguez-Escales, Paula; Folch, Albert; van Breukelen, Boris M.; Vidal-Gavilan, Georgina; Sanchez-Vila, Xavier

DOI

[10.1016/j.jhydrol.2016.04.012](https://doi.org/10.1016/j.jhydrol.2016.04.012)

Publication date

2016

Document Version

Accepted author manuscript

Published in

Journal of Hydrology

Citation (APA)

Rodríguez-Escales, P., Folch, A., van Breukelen, B. M., Vidal-Gavilan, G., & Sanchez-Vila, X. (2016). Modeling long term Enhanced in situ Biotenitrification and induced heterogeneity in column experiments under different feeding strategies. *Journal of Hydrology*, 538, 127-137. <https://doi.org/10.1016/j.jhydrol.2016.04.012>

Important note

To cite this publication, please use the final published version (if applicable).
Please check the document version above.

Copyright

Other than for strictly personal use, it is not permitted to download, forward or distribute the text or part of it, without the consent of the author(s) and/or copyright holder(s), unless the work is under an open content license such as Creative Commons.

Takedown policy

Please contact us and provide details if you believe this document breaches copyrights.
We will remove access to the work immediately and investigate your claim.

Modelling long term Enhanced *in situ* Bionitrification and induced heterogeneity in column experiments under different feeding strategies

Paula Rodríguez-Escales^{1,2*}, Albert Folch^{1,3}, Boris M. van Breukelen⁴, Georgina Vidal-Gavilan^{2,5}, Xavier Sanchez-Vila¹

¹Hydrogeology Group (GHS), Department of Civil and Environmental Engineering, Universitat Politècnica de Catalunya (UPC), c/Jordi Girona 1-3, 08034 Barcelona, Spain.

²d D'ENGINY biorem S.L., C. Madrazo 68, 08006 Barcelona, Spain.

³Institut de Ciència i Tecnologia Ambientals (ICTA), Universitat Autònoma de Barcelona (UAB), Bellaterra, Barcelona 08193, Spain

⁴Department of Water management, Faculty of Civil Engineering and Geosciences, Delft University of Technology, Stevinweg 1, Delft, The Netherlands.

⁵Grup de Mineralogia Aplicada i Geoquímica de Fluïds, Departament de Cristal·lografia, Mineralogia i Dipòsits Minerals, Facultat de Geologia, Universitat de Barcelona, Martí Franquès s/n, 08028, Barcelona, Spain.

*Corresponding author: paula.rodriquez.escales@upc.edu

Abstract

Enhanced *In situ* Bionitrification (EIB) is a capable technology for nitrate removal in subsurface water resources. Optimizing the performance of EIB implies devising an appropriate feeding strategy involving two design parameters: carbon injection frequency and C:N ratio of the organic substrate nitrate mixture. Here we model data on the spatial and temporal evolution of nitrate (up to 1.2 mM), organic carbon (ethanol), and biomass measured during a 342 day-long laboratory column experiment (published in Vidal-Gavilan et al., 2014). Effective porosity was 3% lower and dispersivity had a seven-fold increase at the end of the experiment as compared to those at the beginning. These changes in transport parameters were attributed to the development of a biofilm. A reactive transport model explored the EIB performance in response to daily and weekly feeding strategies. The latter resulted in significant temporal variation in nitrate and ethanol concentrations at the outlet of the column. On the contrary, a daily feeding strategy resulted in quite stable and low concentrations at the outlet and complete denitrification. At intermediate times (six months of experiment), it was possible to reduce the carbon load and consequently the C:N ratio (from 2.5 to 1), partly because biomass decay acted as endogenous carbon to respiration, keeping the denitrification rates, and partly due to the induced dispersivity caused by the well-developed biofilm, resulting in enhancement of mixing between the ethanol and nitrate and the corresponding improvement of denitrification rates. The inclusion of a dual-domain model improved the fit at the last days of the experiment as well as in the tracer test performed at day 342, demonstrating a potential transition to anomalous transport that may be caused by the development of biofilm. This modeling work is a step forward to devising

41 optimal injection conditions and substrate rates to enhance EIB performance by minimizing
42 the overall supply of electron donor, and thus the cost of the remediation strategy.

43

1 Introduction

Nitrate is a priority environmental pollutant in many countries due to the combination of high toxicity and widespread presence (European Environment Agency, 2007; Organisation for Economic Co-operation and Development, 2008). Agricultural leaching has been identified as the primary source of groundwater nitrate contamination (Böhlke, 2002; Jahangir et al., 2012). Additional sources of nitrate pollution include landfill leachate, leaking septic tanks, and municipal storm water runoff (Hiscock et al., 1991; Panno et al., 2008).

Different options to reduce the high nitrate concentration levels in groundwater are available, including improved farming practices, delineation of aquifer protection zones, or dilution with low-nitrate water sources. However, these options are seldom available due to legal, logistic, or economical constraints. Thus, groundwater remediation technologies, such as ion exchange, reverse osmosis, electrodialysis, and Enhanced *in situ* Bionitrification (EIB) (Haugen et al., 2002), are often the only practical options left to deal with nitrate-contaminated aquifers.

EIB holds environmental and economic advantages over the other remediation methods mentioned, because it is simple, selective, and cost efficient (Smith et al., 2001). The technology is based on the reduction of nitrate to dinitrogen gas by anaerobic heterotrophic facultative bacteria that use nitrate as electron acceptor. Such bacteria are ubiquitous in soil and groundwater (Beauchamp et al., 1989). EIB is feasible anywhere bacteria may thrive, organic electron donors can be supplied, and oxygen levels are below 1-2 mg/L (Korom, 1992). In natural aquifer conditions, a major limiting factor for

biodenitrification is organic matter. Therefore, the main idea behind EIB is the addition of an organic carbon source (acting as electron donor for nitrate reduction and as a carbon source for biomass growth), while controlling a suite of environmental parameters such as the concentrations of other oxidants (e.g. O₂), pH, and nutrient levels (e.g. phosphorous or oligo-elements). Optimal configuration of EIB, involving the presence of one or more injection and extraction wells, is site specific, depending on pumping rate, groundwater flow velocity, and residence time of nitrate in the system (Khan and Spalding, 2004).

The injection of organic carbon during EIB creates a bioactive zone, characterized by the growth of denitrifier biomass, heterogeneously distributed throughout the porous media depending on nutrient availability. Biomass can be found either as suspended matter or as biofilms attached to the solid matrix. Biofilms occur as micro-colonies or aggregates composed by denitrifier microorganisms, extracellular polymeric or proteinic substances (EPS), and potentially trapped dinitrogen gas formed during denitrification (Dupin and McCarty, 2000; Hand et al., 2008; Rittmann, 1993; Vandevivere and Baveye, 1992).

As biofilm develops and the pore space is occupied, partial bioclogging might take place, affecting a number of hydraulic properties. In addition to bioclogging, a reduction of hydraulic conductivity can be associated with the presence of trapped N₂ gas (Amos and Mayer, 2006; Jarsjö and Destouni, 2000). While the word clogging is traditionally defined in terms of the overall reduction in hydraulic conductivity (Vandevivere and Baveye, 1992), the decrease in effective pore volume caused by biofilm growth also changes porosity. Due to the variation of these two hydraulic parameters, changes in groundwater velocity might be recorded (Pavelic et al., 2007; Taylor and Jaffé, 1990; Taylor et al., 1990), changing residence time between injection and extraction wells, thus influencing the

overall capacity for biodenitrification. Furthermore, the spatial heterogeneity of hydraulic properties caused by the inhomogeneous distribution of biofilm throughout the porous media also promotes changes in dispersivity (Seifert and Engesgaard, 2007). Dispersivity is an important parameter as it affects the mixing of nitrate with injected organic substrate, and it is sometimes the limiting factor for the reaction processes (Dentz et al., 2011).

Thus, the amount of biomass and the way it grows significantly affect the performance of EIB facilities. Biomass growth is driven among other things by the feeding strategy, i.e., the frequency of injection, the total carbon supplied, and the resulting carbon-nitrogen ratio (C:N). With the objective of limiting the biomass growth, some authors suggested injecting the electron donor in discrete pulses rather than as a continuous supply (Franzen et al., 1997; Gierczak et al., 2007; Peyton, 1996; Semprini et al., 1991; Semprini et al., 1990; Shouche et al.). Nevertheless, little is known about how the frequency of injection pulses affects biomass growth and nitrate degradation. Regarding the C:N ratio, Vidal-Gavilan et al. (2014) observed that even working with low C:N ratios (C:N=1; below the stoichiometric one: C:N = 2.5), high denitrification rates were achieved after biofilm development. The authors attributed this to the occurrence of endogenous bacterial decay.

Proper understanding of processes occurring during EIB involves the need for multispecies reactive transport modeling (RTM) (Chen and MacQuarrie, 2004; Lee et al., 2006; Rodríguez-Escales et al., 2016). Such models can facilitate exploring a variety of remediation strategies such as injection duration and rate, and concentration of reactants. Nevertheless, there is a need to develop specific models to evaluate how different feeding strategies interact with transport processes.

The present work is aimed at developing a model capable of reproducing different feeding injection frequencies (from weekly to daily) with different C:N ratios in a long term column experiment of Enhanced *in situ* Biotenitrification, lasting 342 days (Vidal-Gavilan et al., 2014). This modeling study focusses on the EIB performance in response to the frequency of organic substrate addition as well as the changes in hydraulic and transport properties promoted by the growth of biofilm. Proper understanding of the processes taking place allow defining the optimal injection strategy (frequency and rate) capable of enhancing EIB performance (high performance at low cost) by minimizing the overall supply of labile organic carbon substrate.

2 Materials and Methods

2.1 Description of the experiment and data set

A full description of the experiment is provided in Vidal-Gavilan et al. (2014), and sketched here in Figure 1 for completeness. It consisted of a glass cylindrical column (70 cm length, 8 cm inner diameter) filled with unconsolidated sediment from a sandy alluvial aquifer (located in Argenton, NE Spain). The sediment was composed by medium and coarse-grained sand mainly made up of quartz and feldspar and with a small silt content, the organic matter content in the sediment was negligible (Vidal-Gavilan et al., 2014). Water was forced to flow from the bottom to the top of the column with a pump-controlled average flow-rate of 180 mL/d resulting in a residence time in the column of about 6.4 days. A total of eight sampling ports were installed: one at the inflow reservoir, six along the column (at 6, 16, 26, 36, 46 and 56 cm from inlet), and one at the outflow, allowing the delineation of aqueous compounds and suspended biomass profiles at different predefined

times. The data set provided in Vidal-Gavilan et al. (2014) and used in the modeling effort includes aqueous concentrations of ethanol, nitrate, and biomass at selected times at the sampling ports placed within the column. A control experiment without carbon substrate addition ran for 2 months, and natural denitrification was not observed, as changes in nitrate along the column were lower than 1% (Vidal-Gavilan et al., 2014).

The water used in the experiment was obtained from an existing large-diameter well located at the site. Three 25-L containers were used to store the input water for the experiment, filled up at different days (August 2011, December 2011, and April 2012). The well was always purged prior to sampling. No forced deoxygenation took place, so that the input water (see Table 1) was oxic and saturated with oxygen. The experiment ran for 342 days at aquifer temperature (15°C). Ethanol was added as an external organic carbon source by means of four injectors located 16 cm from the inlet (see Figure 1). It was added by mixing it with the input water previous to injection (Table 1). Different feeding strategies were tested during the experiments (Table 2), characterized by different injection frequencies (weekly *versus* daily) and carbon to nitrogen molar ratios (from 2.5 to 1). In this ratio the amount of C is computed from the concentration of ethanol multiplied with the duration of injection (0.5 min). Feeding was twice discontinued, first between days 150 and 175 due to pump failure (no water was supplied), and then between days 286 and 311, this time to evaluate the resilience of the system to the absence of feeding (water with no ethanol was supplied during that second period).

Two tracer tests were performed, one previous to the start of the experiment, before any feeding took place, and a second one at day 342. The tests were conducted under continuous flow with constant concentration of bromide (1.45 and 2.23 mM, respectively).

During the two tracer tests the flow rate was 835 mL/d. The bromide breakthrough curves were monitored at the outflow point.

2.2 Model construction

Here we describe first the biogeochemical equations used in the biodenitrification model; second, the hydrogeological parameters derived from the two tracer tests; third, the codes used in the modeling effort; and fourth, the calibration process.

2.2.1 EIB biogeochemical model

Biodenitrification was modelled considering both nitrate respiration and biomass growth (see e.g., Rodríguez-Escales et al., 2014). The reactions considered are:

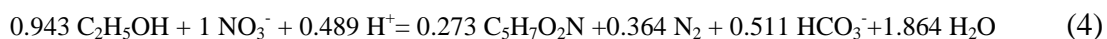
$$r_{ED} = -k_{max} \frac{[ED]}{[ED] + K_{S,ED}} \frac{[EA]}{[EA] + K_{S,EA}} [X] \quad (1)$$

$$r_{EA} = Qr_{ED} - Sb[X] \quad (2)$$

$$r_X = -Y_h r_{ED} - b[X] \quad (3)$$

where [ED] is the concentration of the electron donor (ethanol, C_2H_5OH); [EA] that of the electron acceptor (nitrate), and [X] the denitrifier biomass concentration, all expressed in $[ML^{-3}]$; $k_{max} [T^{-1}]$ is the consumption rate of electron donor per unit value of biomass; $K_{S,ED} [ML^{-3}]$ and $K_{S,EA} [ML^{-3}]$ the half saturation constants of electron donor and acceptor, respectively; $b [T^{-1}]$ a biomass decay constant; Y_h the microbial yield $[C \text{ biomass} / C \text{ ethanol}]$, and $Q [N \text{ nitrate} / C \text{ ethanol}]$ and $S [N \text{ nitrate} / C \text{ endogenous}]$. Both K_{max} (μ_{max}/Y_h) and K_s were fitting parameters, whereas S and Q were stoichiometric factors

determined by the driving denitrification reaction (4). Biomass was conceptualized as having an average chemical composition of $C_5H_7O_2N$ (Porges et al., 1956).



Equation (4) was determined following the instructions of Rittmann and McCarty (2001) and it applies to the following determined parameter values: (i) the portion of substrate (ethanol) used for cell synthesis during denitrification (Y_h) was 0.724 C-biomass/C-ethanol (in agreement with Rodríguez-Escales et al. 2014); and (ii) the portion of nitrate consumed by substrate oxidation (Q) was 0.53 mol nitrate-mol C-ethanol. The stoichiometric relationship between nitrate and endogenous carbon (S) was 0.92 mol nitrate-mol C endogenous, following (Rodríguez-Escales et al., 2014).

Although the injected solution was partly to almost fully oxic (oxygen concentrations measured varied between 0.06 and 0.2 mM), ethanol oxidation by oxygen was and could be neglected. This assumption was based on ethanol consumption by oxygen being between 0.1 and 4% of ethanol injected (depending on initial concentrations). Moreover, preliminary models considering instantaneous reduction of oxygen showed that oxygen was consumed within the first 5 cm of the column (results not shown). Considering all of this and in order to simplify the model, ethanol oxidation by oxygen was not contemplated.

Nitrite accumulation was not relevant in the experiment (only present during the first 20 d, in concentrations below 0.1 mM; whereas nitrate decreased then with 1.2-1.6 mM.). Therefore, the model contemplates only one step reduction from nitrate to dinitrogen gas. The potential accumulation of NO and N_2O was discarded because the system was maintained at low oxygen concentrations, with enough labile organic carbon, and with pH

values between 7 and 8; under these conditions complete denitrification is expected (Rivett et al., 2008; Tallec et al., 2008).

Most often, the amount of bacteria suspended in the aqueous phase is quite small as compared to that attached to the aquifer matrix (Barry et al., 2002; Rittmann, 1993). As a way to implement a practical model, minimizing the number of fitting parameters, we assumed that all biomass was attached to the solid matrix, and thus immobile, without considering attachment and detachment processes, described for example in Clement et al. (1997). The initial biomass concentration was estimated in 6.5×10^{-8} mmol/kg, considering a most probable number for denitrifying cells equal to 37.5 cel/ml (Vidal-Gavilan et al. 2014) and converted to moles using a denitrifier cell weight of 10^{-9} mg (Alvarez et al., 1994). The initial value used in PHT3D was normalized by liter of water.

Finally, the column was considered as an open system in equilibrium with the atmosphere because it was open at its upper part. Thus, degassing was allowed if the sum of partial pressures of gases (mainly dinitrogen gas and carbon dioxide) exceeded the atmospheric pressure. Prior to the simulation process, and in order to evaluate the potential hydraulic conductivity variations due to bubble formation, we evaluated the potential building up of denitrification gases. Thus, we ran the model under closed system conditions. The results showed that the hydrostatic pressure was exceeded in most feeding strategies illustrating that degassing could occur. To limit the chance for gas entrapment, which would be the main responsible of changes in hydraulic conductivity (Amos and Mayer, 2006), we purposely ran the column experiment in vertical mode with water flowing upwards. In this way, gas entrapment should have been limited as any gas formed could escape at the top outlet of the column and the flow of gas bubbles and water in the

column were aligned. Furthermore, we expect that the coarse sand (grain size between 1 and 2 mm) used in the column further limited any gas entrapment.

2.2.2 Transport model parameters evaluated from the tracer tests

Two tracer tests with a conservative tracer (Br⁻) were performed at days 0 and 342 in order to build a conceptual model for conservative transport and to estimate the corresponding hydraulic parameters. Invoking the parsimony principle, we first tried to fit the breakthrough curves with the simplest model, that of the one-dimensional advection-dispersion equation (ADE).

The ADE model could properly reproduce the test performed at time 0, but failed to fit the tail of the experimental BTC obtained during the second test at day 342. As an alternative model we selected a dual porosity model (Delay et al., 2013; Haggerty and Gorelick, 1995; Lawrence et al., 2002; Seifert and Engesgaard, 2007), representing the porous medium as composed of a mobile and of an immobile region that coexist at any given point in the domain. The first one was an aqueous phase where advection and dispersion were the main transport processes, whereas the second one was a (diffusion zone governed by biofilm dynamics). Both regions exchange mass proportionally to the difference in their concentrations at any given time. The equation describing the concentration of species *i* in the mobile zone, $c_{m,i}$, is:

$$\phi_m \frac{\partial C_{m,i}}{\partial t} = -q \frac{\partial C_{m,i}}{\partial x} + \phi_m \frac{D \partial^2 C_{m,i}}{\partial x^2} - \Gamma_i \quad (5)$$

where *D* is the dispersion coefficient, *q* is Darcy's velocity, ϕ_m the porosity corresponding to the mobile zone (aqueous phase with aqueous solution), and Γ_i the source-sink term

controlling the mass transfer of species i between the mobile (m) and the immobile regions (im) (biofilm phase with microorganisms attached to the sediment), given by:

$$\Gamma_i = \alpha \phi_{im} (C_{m,i} - C_{im,i}) \quad (6)$$

with α the mass transfer rate [T^{-1}], ϕ_{im} [-] the porosity associated with the immobile region (volume fraction occupied by the biofilm), and $C_{im,i}$ the concentration of species i in the immobile region. The actual total porosity is $\phi_t = \phi_m + \phi_{im}$, and remains constant during biofilm formation. The rationale behind it is that the biofilm colonizes pores that were initially occupied by water in sediments not affected by consolidation or swelling, so that the sediment occupied the same volume at the beginning and end of the experiment. A key parameter characterizing the shape of the BTC in the dual porosity model is the ratio of porosities (Fernàndez-Garcia and Sanchez-Vila, 2015) given by:

$$\beta = \frac{\phi_{im}}{\phi_m} = \frac{\phi_t}{\phi_m} - 1 \quad (7)$$

2.2.3 Used codes and calibration process

The PHT3D model code (v. 2.17) (Prommer and Post, 2010) was used to simulate the evolution of groundwater hydrochemistry during enhanced biodenitrification in the column. This model couples the transport simulator MT3DMS (Zheng and Wang, 1999) and the geochemical model PHREEQC-2 (Parkhurst and Appelo, 1999), by means of a sequential split-operator technique. Regarding solute transport, PHT3D incorporates either the traditional ADE, or else the dual domain model through MT3DMS. Since the PHT3D reaction module uses the original PHREEQC-2 database syntax, equilibrium and non-equilibrium reaction chains can be defined. For reactions in equilibrium, the constants were

taken directly from the database. Kinetic reactions such as ethanol degradation and bacterial growth/decay (1-3), not being part of the standard database, were incorporated into the module in the form of BASIC routines, as explained in Rodríguez-Escales et al. (2014) and Carrey et al. (2014).

Regarding the tracer tests, the interpretation using the traditional ADE and the dual domain model was carried out with the CXTFIT code (Toride et al., 1999). We developed the inverse modelling of transport processes using the experimental information of the BTCs from the tracer tests and we determined the following parameters: dispersivity coefficient, total, mobile and immobile porosities, and, dual domain transfer coefficient. Furthermore, CXTFIT provides the confidence interval (95%) of each parameter as well as their corresponding standard deviations. In order to avoid the correlation between immobile porosity and dispersivity coefficient in the transport equation (e.g. Wehrer et al. 2012), the calibration process was divided in two steps. First of all, we calibrated the dispersivity coefficient and the mobile porosity without considering the tail. Then, we incorporated the dual domain model to improve the fittings of the tail, allowing an independent estimation of the immobile porosity. Following this methodology, we only related the dispersivity to the change into the geometry and not also to the diffusion processes avoiding its correlation with immobile porosity.

To assist the biodenitrification model calibration process, the model independent parameter estimation program PEST (Doherty, 2005) was coupled to PHT3D and used to estimate the reaction rate parameters (k_{\max} , $K_{S,ED}$, $K_{S,EA}$, and b). PEST computed the sensitivities, correlations, and linear uncertainties (confidence intervals) of the optimized model parameters. For the calibration process, the error associated with the measurement

was treated as 95% confidence interval, and weights were applied using the inverse of the standard deviation of this confidence interval (Karlsen et al., 2012). Using this method, values with a higher accuracy get assigned a higher weight and the resulting objective function became dimensionless. Standard ranges for measurement error of chemical sampling were given with an accuracy of 5%. Weights (w) for each chemical species observation i were thus calculated:

$$w_i = \frac{1.96}{\varepsilon_i C_i} \quad (8)$$

where ε is the measurement error described above and C is the observed concentration. For the calibration process, we used the experimental data of nitrate during the first 100 days of the experiment (35 points). The calibration process of the reactive transport was performed by fixing the conservative transport parameters. Finally, we also evaluated the likelihood of the models comparing the Akaike information criterion values (AIC) calculated by PEST.

3 Results and discussion

3.1 Tracer tests interpretation: derivation of transport processes and parameters

The first step is the interpretation of the 1-D conservative tracer tests. The traditional ADE equation was capable of properly fitting the curve corresponding to the first test, but it failed to provide a good fit of the tail of the BTC corresponding to the second test, with a maximum error in estimated concentrations of 3%. On the other hand, the dual domain model was capable to reproduce the tail of the BTC corresponding to the second test indicating a transition from a Fickian description of transport at the start to an anomalous description of transport at the end of the EIB experiment. The reported BTCs are presented

in Figure 2, together with the best fits obtained either with code CTXFIT at day 0 (single porosity) and at day 342 (dual porosity); the fitted parameters are listed in Table 3. Groundwater velocity was very similar in the two tests (see Table 3). The hydraulic gradient could not be measured in the applied experimental setup. Therefore, any reduction in hydraulic conductivity due to biofilm growth could not be assessed. Total (single-phase) porosity and dispersivity were estimated from the first test; total porosity, the proportion of immobile and mobile porosity, dispersivity, and the mass transfer rate were estimated from the second one. Total porosity values estimated from both tests were statistically not different, with best estimates of 0.33 ± 0.03 to 0.34 ± 0.05 , and estimation intervals largely overlapping (Table 3). However, the dual porosity model estimated an immobile porosity of 0.015 ± 0.009 at day 342.

There was a remarkable seven-fold increase in the dispersivity coefficient estimated from the two tests, with the mean value changing from 0.48 ± 0.01 to 3.44 ± 0.25 cm (see Table 3). This result is consistent with the observations by Taylor and Jaffé (1990) who also described an increase in immobile porosity linked to an increase in dispersivity in a column experiment colonized by biomass. Several studies also report significant changes in dispersivity, ranging from two- to eight-fold increases, in bioremediation experiments lasting 2-7 weeks (Arnon et al., 2005; Bielefeldt et al., 2002; Hill and Sleep, 2002; Seifert and Engesgaard, 2007; Sharp et al., 1999; Taylor and Jaffé, 1990; Taylor et al., 1990), and as high as a 10-100 fold variation for long duration experiments (Taylor and Jaffé, 1990; Bielefeldt et al., 2002). This increase in dispersivity is generally associated to denitrifier biomass colonizing the sand grains forming the soil skeleton. Thus, while total porosity remained basically constant, a small fraction was colonized by biomass aggregates and

micro-colonies, changing its behavior from water accessible by flow (mobile) to inaccessible (immobile). Such aggregates have been reported to induce irregular surfaces of the solid particles (Rittmann, 1993), and consequently, to increase the heterogeneity in the pore size distribution (Seifert and Engesgaard, 2007), thus enhancing dispersivity.

The change in the conceptual model of transport was associated with the growth of biofilm during the duration of the experiment. Thus, the fitted parameters of the dual domain model have a clear physical explanation; for example, the calibrated α parameter ($\alpha = 0.019 \pm 0.018 \text{ d}^{-1}$) can be interpreted as the inverse of the characteristic diffusive time of bromide transport through the immobile phase (thus being equal to 45 days). Moreover, the β value ($\beta = 0.046 \pm 0.030$) represented the proportion of the void volume occupied by the biofilm ($4.65 \pm 2.96 \%$).

Regarding the calibration process of the transport parameters, the automatic calibration showed that during the two steps of calibration the parameters were not correlated because the correlation coefficients were lower than 0.95 (Hill et al., 1998). During the first step (calibration using ADE of velocity and dispersion), the correlation among parameters was lower than 0.025 for the two tracer tests. During the second step, the correlation between immobile porosity and the mass transfer coefficient was 0.21. The coefficients of variation (CV) of the parameters of ADE were well estimated, as their values were generally low (less than 0.15). Regarding the parameters of the dual domain model, they were estimated as highly uncertain.

3.2 Long-term modeling of EIB. Impact of organic carbon injection strategies

Based on tracer tests results the column experiment was first interpreted using a Fickian representation of transport, i.e., based on the ADE. Emphasis was placed on the performance of the daily and weekly feeding strategies upon the observed temporal evolution of the concentrations of nitrate, ethanol, and biomass. Since Table 3 displays two dispersivity values corresponding to days 0 and 342, but no intermediate values were obtained, the 342-day column experiment was modeled using both dispersivity values, by assuming that they lasted the full duration of the experiment, thus providing two limiting cases. The column was discretized into 70 elements of 1 cm length. The time discretization was selected to satisfy Peclet and Courant criteria. Dispersive transport was computed by the third-order Total Variation Diminishing solution, a feature available in PHT3D.

The actual data and the fittings with the two dispersivity values are shown in Figure 3. Neither porosity (obtained from the tracer test, 0.33), nor the geochemical parameters of reactions in equilibria (selected from the PHREEQC2 database) were calibrated. The only calibrated parameters were the microbiological ones (Table 4) and, all were in range compared to values reported in the literature. Note that we compared the μ_{\max} parameter instead the k_{\max} with literature values, because it only depends on velocity reaction and it is easier to compare. The automatic calibration procedure used for the estimation of kinetic parameters in the denitrification model showed that the evaluated parameters were not cross-correlated, as indicated by their values in the coefficient correlation matrix being below 0.747 (data not shown). That is, given the available observations for model calibration, each model parameter affected the simulated equivalents to the observations sufficiently differently. The values of the coefficients of variation, CVs, were relatively

high, ranging from 0.26 to 0.61. As pointed out by Greskowiak et al. (2005), large CVs do not necessarily imply an incorrect model concept. Instead, it may indicate that the available observation data are insufficient to uniquely constrain (estimate) the parameter, or that there is an underlying physical basis for relatively high CVs.

The lowest dispersivity value (0.48 cm) resulted in a good fitting of the experimental data during the weekly feeding strategy (Figure 3), lasting the first 98 days, indicating that during this period dispersivity did not change significantly. This result is in contrast with other works based on column experiments using somewhat different experimental conditions like organic substrate but were all fed continuously (Bielefeldt et al., 2002; Seifert and Engesgaard, 2007; Taylor and Jaffé, 1990) (Table 5). For example, Seifert and Engesgaard (2007), using acetate and oxygen as electron acceptor, reported an increase in dispersivity from 0.33 cm to 1.1 cm in 64 days. On the other hand, Bielefeldt et al. (2002), in an experiment on propylene glycol degradation using nitrate as electron acceptor, observed a 20-60 fold increase in 15 days in clean sand. Finally, Delay et al. (2013) reported a noticeable change in dispersivity in a 1.4 day column denitrification experiment. In short, from the data in Table 5, it seems that a weekly feeding strategy limits dispersivity increases with time.

We note that Figure 4 reports the modeling results assuming a constant representative dispersivity value all throughout the column. We expect though that most of the biomass colonization took place around the injection point (Kildsgaard and Engesgaard, 2001), associated with the highest EA and ED concentrations and, consequently, the modification of the transport parameters too. Although the general trends were well captured, the

limitation of considering only one set of transport parameters could explain the discrepancies between the experimental data and the simulated results.

During the daily feeding strategy, starting after day 99, the best overall fit of nitrate concentration was obtained with the final dispersivity value of 3.43 cm. This is visible both for time-series (Figure 3) and for spatial profiles (Figure 4). Consequently, the increase in dispersivity seems triggered by the changes in feeding strategy, from weekly to daily pulses. During weekly injection, biomass was not fed homogenously, and probably biomass growth was through colonies or aggregates that did not colonizing the whole sandy media. On the other hand, daily injection drove a more continuous growth of biomass (probably in biofilm form) and favoring the colonization of the whole column (Rittmann, 1993). We thus contend that induced heterogeneity was larger in the daily scenario as compared to the weekly one, and consequently, a seven-fold increase of dispersivity in the former feeding strategy was observed. This increase was smaller than others reported in the literature for continuous feeding (see Table 5 for values and references). This can be explained because the injection was performed in the form of a daily pulse, rather than fully continuous. Besides this change in feeding strategy, the two stop periods in daily feeding strategies could also facilitate the increasing of heterogeneity due to the detachment of biomass and its redistribution through the column (Wehrer et al., 2012). This suggests that both the feeding frequency and the stop periods are key operational parameters that may affect hydraulic parameters and thereby control the transport of chemical species during EIB.

We want to emphasize that the increase of dispersivity was evaluated in a column experiment (1D), thus only considering longitudinal dispersivity. Although it is still unknown how biofilm growth will disturb the dispersivity in 3-D (e.g. field applications),

we would expect an increase in the three directions of dispersivity, longitudinal, and transversal both horizontally and vertically. The last two of those having a most significant impact upon the enhancement of spreading and mixing of nutrients (Chiogna et al., 2012; Rolle et al., 2009).

The biomass concentration decreased corresponding to the low C:N ratios (Figure 3). Note that the biomass concentration did not differ between feeding strategies I and II, indicating that the injection frequency played a lower role than the C:N ratio. Nevertheless, we hypothesize that the biomass growth was different for each strategy. Whereas during weekly feeding strategy, the biomass distribution should not be continuous, in the daily one we should expect that a connected biofilm was formed. This idea follows the observations of Rittmann (1993), who determined that a continuous feeding causes a biofilm whereas a discontinued one resulted in disconnected biomass aggregates. Although the characterization of the attached biomass could be done at the end of the experiment (e.g. Clement et al. (1997)), we recommend for future research the characterization of the biofilm structure through SEM (Scanning Electron Microscope) images.

3.3 The implication of introducing non-Fickianity in the conceptual model

The incorporation of a dual domain transport model resulted in a slight improvement of the model fit from day 183 onwards (Figure 3 and 4, blue dashed-dotted line). The parameters used in the model are reported in Table 3 for transport processes (last row) and Table 4 for the biogeochemical ones. Note that the mass transfer coefficient had a high standard deviation (0.019) in relation to the parameter value (0.018). Considering that, we run the

model with different mass transfer values. The results showed that the model was not very sensitive to this change (results not shown).

As the fit obtained during the weekly feeding strategy by ADE was quite good, much better than the obtained with the non-Fickian model (Figure 3), we contend that during this period the diffusive transport through the biofilm was negligible. Thus, the conceptualization of the porous medium as a dual domain was not considered until the daily feeding strategy started, that supposed to enhance the biofilm developing (conceptualized as immobile porosity). This improvement in fitting is attributed to modeling the partial transformation of initial pores to non-flowing volume (immobile porosity or diffusive layer) that act as electron donor sink. Yet, it is still unknown at which point of the experiment this process was relevant. This could only be assessed by the incorporation of non-invasive techniques to monitor biofilm evolution in future studies. We emphasize that water velocity conditioned the significance of involving a dual domain into the conceptual transport model. Thus, the impact of a dual domain model in the tracer test interpretation (Figure 2) was more significant than that on the bionitrification experiment (Figure 3-4) because the water velocity was higher (0.5 m/d instead of 0.1 m/d) and thus the time available for mass transfer between the domain was less. Although this difference in velocity, we want to remark that the dual domain model was more likely than the ADE model because its AIC value was the lowest one (203.22 compared to 212.55).

3.4 Significance of the C:N ratio and implications for EIB design

In the scenarios with the lowest C:N ratios (strategies III, days 206-252 and IV, days 253-342), the model correctly reproduces the experimental data of nitrate and ethanol being

completely consumed inside the column (not detected at the outlet). This means that the source of organic carbon was used optimally, fully consumed, as opposed to that observed in strategy I. Note that the increase in dispersivity resulted in enhanced spreading and then mixing of the injected ethanol with nitrate, enabling a more efficient substrate use.

Another parameter that helped defining the success of the different injection strategies is the stress produced upon the biomass population. When the carbon load was reduced (strategies III and IV), the modeled biomass diminished (see Figure 3). However, nitrate remained undetected, indicating that denitrification was partially linked to biomass decay (endogenous respiration) meaning that there was not enough external carbon to maintain the large biomass population (see Figure 5). The use of endogenic carbon as electron donor in bioremediation facilities has already been reported in other works (Béranger et al., 2006; Rodríguez-Escales et al., 2016). The decrease in biomass concentration indicated that the low C:N strategies were not sustainable in time. Nevertheless, working with low C:N could be a good tool to reduce the risk of clogging.

Besides this, the amount of ethanol used in these strategies was lower than in strategies I and II (Figure 6), which would imply important savings (the main cost in an EIB operation is electron donor injection). A proper design of the amount of carbon supplied could represent significant savings in an EIB technology. For these reasons, we recommend applying low C:N strategies when the system has reached maturity (complete denitrification achieved, mature biofilm, no nitrite accumulation) and/or when an important risk of clogging exists (monitored with continuous or semi continuous measurement of hydraulic conductivity and mobile porosity).

4 Summary and conclusions

An Enhanced *In situ* Biotenitrification experiment, performed in a 70 cm long column under virtually constant flow rate and different feeding strategies was modeled. Injection strategies were defined in terms of periodicity of injection of organic carbon (ethanol), and thus resulting C:N ratio. A long term reactive transport (342 d) model based on the Advection Dispersion Equation (ADE) fitted properly most of the experimental data.

Throughout the experiment, estimated dispersivity varied from the beginning to the end of the experiment. During the weekly supply strategy I (first 98 days), the best fit was obtained using a low dispersivity value (0.48 cm), whereas during the daily strategy, it was best fitted with a larger dispersivity value (3.43 cm). We attributed this increase to the change in injection periodicity, from weekly to daily, after day 98, resulting in biofilm growth. Furthermore, after day 252, with a very mature system, data fitted better using a dual-domain model (i.e., non-Fickian) as compared to one based on the ADE. This change was associated with the presence of a diffusive layer (biofilm) increasing its relevance with time. Although the dynamic conditions of the system, the presented model has been capable of reproducing satisfactorily the experimental observations in all feeding strategies.

On the other hand, reducing the C:N ratio below the stoichiometric requirements allowed the optimization of ethanol injection into the system avoiding its presence at the column outlet. At this point, biomass decay increased and the endogenous carbon acted as partial source of electron donor during the denitrification process. Nevertheless, the decrease of modelled biomass concentration in time showed that this strategy is not

sustainable at long term and that it only can be used when a mature biofilm exists in the subsurface.

Our work has shown that besides other parameters (nutrient loading, flow rate, or grain size), injection frequency is a significant operational parameter that can affect a number of hydraulic parameters, notably dispersivity. This finding could be extended to promote field Enhanced *In Situ* Bionitrification (EIB) applications. A larger dispersivity value offers the possibility of enhancing spreading of injected solutes, increasing the area treated per injection point and limiting the organic carbon loss in this particular *in situ* technique. Thus, this will promote the growth of biofilm and, when a mature system is eventually reached, reducing the C:N ratio can minimize the risk of clogging. So, in order to improve efficiency and saving costs in real field scale applications, feeding strategy in terms of frequency and C:N relationship should be evaluated before the design and construction of EIB installations, as well as during its operation.

Acknowledgements

We thank the three reviewers and the associate editor for their comments and suggestions, which helped improve the quality of the manuscript. This work was financed by projects CGL2011-29975-C04-01/04, and CSD2009-00065 Consolider-SCARCE project from the Spanish Government, as well as projects 2014-SGR-1377 and TEM-2009 from the Catalan Government, and MARSOL FP7-ENV-2013-WATER-INNO-DEMO from the EU. XS acknowledges support from the ICREA Academia Program.

References

- Alvarez, P., Anid, P., Vogel, T., 1994. Kinetics of Toluene Degradation by Denitrifying Aquifer Microorganisms. *J. Environ. Eng.*, 120(5): 1327-1336. DOI:10.1061/(ASCE)0733-9372(1994)120:5(1327)
- Amos, R.T., Mayer, K.U., 2006. Investigating the role of gas bubble formation and entrapment in contaminated aquifers: Reactive transport modelling. *J. Contam. Hydrol.*, 87(1-2): 123-154. DOI:<http://dx.doi.org/10.1016/j.jconhyd.2006.04.008>
- Arnon, S., Adar, E., Ronen, Z., Yakirevich, A., Nativ, R., 2005. Impact of microbial activity on the hydraulic properties of fractured chalk. *J. Contam. Hydrol.*, 76(3-4): 315-36. DOI:10.1016/j.jconhyd.2004.11.004
- Barry, D.A. et al., 2002. Modelling the fate of oxidisable organic contaminants in groundwater. *Adv. Water Resour.*, 25(8-12): 945-983. DOI:10.1016/S0309-1708(02)00044-1
- Beauchamp, E.G., Trevors, J.T., Paul, J.W., 1989. Carbon Sources for Bacterial Denitrification. In: Stewart, B.A. (Ed.), *Adv. Soil. Sci.* Springer New York, pp. 113-142. DOI:10.1007/978-1-4613-8847-0_3
- Bielefeldt, A., McEachern, C., Illangasekare, T., 2002. Hydrodynamic Changes in Sand due to Biogrowth on Naphthalene and Decane. *J. Environ. Eng.*, 128(1): 51-59. DOI:10.1061/(ASCE)0733-9372(2002)128:1(51)
- Béranger, S., Sleep, B., Sherwood Lollar, B., Brown, A., 2006. Isotopic Fractionation of Tetrachloroethene Undergoing Biodegradation Supported by Endogenous Decay. *J. Environ. Eng.*, 132(7): 725-735. DOI:10.1061/(ASCE)0733-9372(2006)132:7(725)
- Böhlke, J.-K., 2002. Groundwater recharge and agricultural contamination. *Hydrogeol. J.*, 10(1): 153-179. DOI:10.1007/s10040-001-0183-3

- Carrey, R. et al., 2014. Nitrate attenuation potential of hypersaline lake sediments in central Spain: Flow-through and batch experiments. *J. Contam. Hydrol.*, 164(0): 323-337. DOI:<http://dx.doi.org/10.1016/j.jconhyd.2014.06.017>
- Chen, D.J.Z., MacQuarrie, K.T.B., 2004. Numerical simulation of organic carbon, nitrate, and nitrogen isotope behavior during denitrification in a riparian zone. *J. Hydrol.*, 293(1-4): 235-254. DOI:10.1016/j.jhydrol.2004.02.002
- Chiogna, G., Hochstetler, D.L., Bellin, A., Kitanidis, P.K., Rolle, M., 2012. Mixing, entropy and reactive solute transport. *Geophysical Research Letters*, 39(20): L20405. DOI:10.1029/2012GL053295
- Clement, T.P., Peyton, B.M., Skeen, R.S., Jennings, D.A., Petersen, J.N., 1997. Microbial growth and transport in porous media under denitrification conditions: experiments and simulations. *J. Contam. Hydrol.*, 24(3-4): 269-285. DOI:[http://dx.doi.org/10.1016/S0169-7722\(96\)00014-9](http://dx.doi.org/10.1016/S0169-7722(96)00014-9)
- Delay, F., Porel, G., Chatelier, M., 2013. A dual flowing continuum approach to model denitrification experiments in porous media colonized by biofilms. *J. Contam. Hydrol.*, 150(0): 12-24. DOI:<http://dx.doi.org/10.1016/j.jconhyd.2013.04.001>
- Dentz, M., Le Borgne, T., Englert, A., Bijeljic, B., 2011. Mixing, spreading and reaction in heterogeneous media: A brief review. *J. Contam. Hydrol.*, 120-121(0): 1-17. DOI:<http://dx.doi.org/10.1016/j.jconhyd.2010.05.002>
- Doherty, J., 2005. PEST: model independent parameter estimation. Watermark Numerical Computing, fifth edition of user manual.
- Dupin, H.J., McCarty, P.L., 2000. Impact of Colony Morphologies and Disinfection on Biological Clogging in Porous Media. *Environ. Sci. Technol.*, 34(8): 1513-1520. DOI:10.1021/es990452f
- European Environment Agency, E., 2007. Present concentration of nitrate in groundwater bodies in European countries, 2003.

573 Fernàndez-Garcia, D., Sanchez-Vila, X., 2015. Mathematical equivalence between time-dependent
 574 single-rate and multirate mass transfer models. *Water Resour. Res.*, 51(5): 3166-3180.
 575 DOI:10.1002/2014WR016348

576 Franzen, M.E.L., Petersen, J.N., Clement, T.P., Hooker, B.S., Skeen, R.S., 1997. Pulsing of
 577 multiple nutrients as a strategy to achieve large biologically active zones during in situ
 578 carbon tetrachloride remediation. *Comput. Geosci.*, 1(3): 271-288.
 579 DOI:10.1023/A:1011573429996

580 Gierczak, R., Devlin, J.F., Rudolph, D.L., 2007. Field test of a cross-injection scheme for
 581 stimulating in situ denitrification near a municipal water supply well. *J. Contam. Hydrol.*,
 582 89(1–2): 48-70. DOI:<http://dx.doi.org/10.1016/j.jconhyd.2006.08.001>

583 Greskowiak, J., Prommer, H., Vanderzalm, J., Pavelic, P., Dillon, P., 2005. Modeling of carbon
 584 cycling and biogeochemical changes during injection and recovery of reclaimed water at
 585 Bolivar, South Australia. *Water Resour. Res.*, 41(10): W10418.
 586 DOI:10.1029/2005WR004095

587 Haggerty, R., Gorelick, S., 1995. Multiple-Rate Mass Transfer for Modeling Diffusion and Surface
 588 Reactions in Media with Pore-Scale Heterogeneity. *Water Resour. Res.*, 31(10): 2383-2400.
 589 DOI:10.1029/95WR10583

590 Hand, V.L., Lloyd, J.R., Vaughan, D.J., Wilkins, M.J., Boulton, S., 2008. Experimental studies of the
 591 influence of grain size, oxygen availability and organic carbon availability on bioclogging
 592 in porous media. *Environ. Sci. Technol.*, 42(5): 1485-91.

593 Haugen, K.S., Semmens, M.J., Novak, P.J., 2002. A novel in situ technology for the treatment of
 594 nitrate contaminated groundwater. *Water Res.*, 36(14): 3497-3506.
 595 DOI:[http://dx.doi.org/10.1016/S0043-1354\(02\)00043-X](http://dx.doi.org/10.1016/S0043-1354(02)00043-X)

596 Hill, D.D., Sleep, B.E., 2002. Effects of biofilm growth on flow and transport through a glass
 597 parallel plate fracture. *J. Contam. Hydrol.*, 56(3-4): 227-46.

- Hill, M.C., Cooley, R.L., Pollock, D.W., 1998. A Controlled Experiment in Ground Water Flow Model Calibration. *Ground Water*, 36(3): 520-535. DOI:10.1111/j.1745-6584.1998.tb02824.x
- Hiscock, K.M., Lloyd, J.W., Lerner, D.N., 1991. Review of natural and artificial denitrification of groundwater. *Water Res.*, 25(9): 1099-1111. DOI:[http://dx.doi.org/10.1016/0043-1354\(91\)90203-3](http://dx.doi.org/10.1016/0043-1354(91)90203-3)
- Jahangir, M.M.R., Johnston, P., Khalil, M.I., Richards, K.G., 2012. Linking hydrogeochemistry to nitrate abundance in groundwater in agricultural settings in Ireland. *J. Hydrol.*, 448–449: 212-222. DOI:<http://dx.doi.org/10.1016/j.jhydrol.2012.04.054>
- Jarsjö, J., Destouni, G., 2000. Degassing of deep groundwater in fractured rock around boreholes and drifts. *Water Resour. Res.*, 36(9): 2477-2492. DOI:10.1029/2000WR900131
- Karlsen, R.H., Smits, F.J.C., Stuyfzand, P.J., Olsthoorn, T.N., van Breukelen, B.M., 2012. A post audit and inverse modeling in reactive transport: 50 years of artificial recharge in the Amsterdam water supply dunes. *J. Hydrol.*, 454–455(0): 7-25. DOI:<http://dx.doi.org/10.1016/j.jhydrol.2012.05.019>
- Khan, I.A., Spalding, R.F., 2004. Enhanced in situ denitrification for a municipal well. *Water Res.*, 38(14–15): 3382-3388. DOI:<http://dx.doi.org/10.1016/j.watres.2004.04.052>
- Kildsgaard, J., Engesgaard, P., 2001. Numerical analysis of biological clogging in two-dimensional sand box experiments. *J. Contam. Hydrol.*, 50(3–4): 261-285. DOI:[http://dx.doi.org/10.1016/S0169-7722\(01\)00109-7](http://dx.doi.org/10.1016/S0169-7722(01)00109-7)
- Korom, S.F., 1992. Natural denitrification in the saturated zone: A review. *Water Resour. Res.*, 98(6). DOI:doi:10.1029/92WR00252
- Lawrence, A.E., Sanchez-Vila, X., Rubin, Y., 2002. Conditional moments of the breakthrough curves of kinetically sorbing solute in heterogeneous porous media using multirate mass transfer models for sorption and desorption. *Water Resour. Res.*, 38(11): 1248. DOI:10.1029/2001WR001006

624 Lee, M.-S., Lee, K.-K., Hyun, Y., Clement, T.P., Hamilton, D., 2006. Nitrogen transformation and
 625 transport modeling in groundwater aquifers. *Ecol. Modell.*, 192(1–2): 143-159.
 626 DOI:10.1016/j.ecolmodel.2005.07.013
 627 Organisation for Economic Co-operation and Development, O., 2008. Environmental performance
 628 of agriculture in OECD countries since 1990.
 629 Panno, S.V., Kelly, W.R., Hackley, K.C., Hwang, H.-H., Martinsek, A.T., 2008. Sources and fate of
 630 nitrate in the Illinois River Basin, Illinois. *J. Hydrol.*, 359(1–2): 174-188.
 631 DOI:<http://dx.doi.org/10.1016/j.jhydrol.2008.06.027>
 632 Parkhurst, D.L., Appelo, C.A.J., 1999. User's guide to PHREEQC (version 2) - a computer program
 633 for speciation, reaction-path, 1D-transport, and inverse geochemical calculations., U.S.
 634 GEOLOGICAL SURVEY.
 635 Pavelic, P. et al., 2007. Water quality effects on clogging rates during reclaimed water ASR in a
 636 carbonate aquifer. *J. Hydrol.*, 334(1–2): 1-16.
 637 DOI:<http://dx.doi.org/10.1016/j.jhydrol.2006.08.009>
 638 Peyton, B.M., 1996. Improved biomass distribution using pulsed injections of electron donor and
 639 acceptor. *Water Res.*, 30(3): 756-758. DOI:[http://dx.doi.org/10.1016/0043-1354\(95\)00220-](http://dx.doi.org/10.1016/0043-1354(95)00220-0)
 640 [0](http://dx.doi.org/10.1016/0043-1354(95)00220-0)
 641 Porges, N., Jasewicz, L., Hoover, S., 1956. Principles of biological oxidation. In biological
 642 treatment of sewage and industrial wastes. Reinhold. Publ., New York.
 643 Prommer, H., Post, V., 2010. A Reactive Multicomponent Transport Model for Saturated Porous
 644 Media. User's Manual. v2.10.
 645 Rittmann, B.E., 1993. The significance of biofilms in porous media. *Water Resour. Res.*, 29(7):
 646 2195-2202. DOI:10.1029/93WR00611
 647 Rittmann, B.E., McCarty, P.L., 2001. Environmental biotechnology : principles and applications.
 648 McGraw-Hill, cop. 2001.

- Rivett, M.O., Buss, S.R., Morgan, P., Smith, J.W.N., Bemment, C.D., 2008. Nitrate attenuation in groundwater: A review of biogeochemical controlling processes. *Water Res.*, 42(16): 4215-4232. DOI:10.1016/j.watres.2008.07.020
- Rodríguez-Escales, P., Folch, A., Vidal-Gavilan, G., van Breukelen, B.M., 2016. Modeling biogeochemical processes and isotope fractionation of enhanced in situ biodenitrification in a fractured aquifer. *Chem. Geol.*, 425: 52-64. DOI:<http://dx.doi.org/10.1016/j.chemgeo.2016.01.019>
- Rodríguez-Escales, P., van Breukelen, B., Vidal-Gavilan, G., Soler, A., Folch, A., 2014. Integrated modeling of biogeochemical reactions and associated isotope fractionations at batch scale: A tool to monitor enhanced biodenitrification applications. *Chem. Geol.*, 365(0): 20-29. DOI:<http://dx.doi.org/10.1016/j.chemgeo.2013.12.003>
- Rolle, M., Eberhardt, C., Chiogna, G., Cirpka, O.A., Grathwohl, P., 2009. Enhancement of dilution and transverse reactive mixing in porous media: Experiments and model-based interpretation. *J. Contam. Hydrol.*, 110(3–4): 130-142. DOI:<http://dx.doi.org/10.1016/j.jconhyd.2009.10.003>
- Seifert, D., Engesgaard, P., 2007. Use of tracer tests to investigate changes in flow and transport properties due to bioclogging of porous media. *J. Contam. Hydrol.*, 93(1–4): 58-71. DOI:<http://dx.doi.org/10.1016/j.jconhyd.2007.01.014>
- Semprini, L. et al., 1991. In-situ biotransformation of carbon tetrachloride under anoxic conditions.
- Semprini, L., Roberts, P.V., Hopkins, G.D., McCarty, P.L., 1990. A Field Evaluation of In-Situ Biodegradation of Chlorinated Ethenes: Part 2, Results of Biostimulation and Biotransformation Experiments. *Ground Water*, 28(5): 715-727. DOI:10.1111/j.1745-6584.1990.tb01987.x
- Sharp, R.R., Cunningham, A.B., Komlos, J., Billmeyer, J., 1999. Observation of thick biofilm accumulation and structure in porous media and corresponding hydrodynamic and mass

674 transfer effects. Water Sci. Technol., 39(7): 195-201. DOI:<http://dx.doi.org/10.1016/S0273->
675 [1223\(99\)00168-7](http://dx.doi.org/10.1016/S0273-1223(99)00168-7)

676 Shouche, M.J., Petersen, J.N., Skeen, R.S., Use of a mathematical model for prediction of optimum
677 feeding strategies for in situ bioremediation. Appl. Biochem. Biotech., 39(1): 763-779.
678 DOI:10.1007/BF02919034

679 Smith, R.L., Miller, D.N., Brooks, M.H., Widdowson, M.A., Killingstad, M.W., 2001. In situ
680 stimulation of groundwater denitrification with formate to remediate. Environ. Sci.
681 Technol., 35(1): 196-203.

682 Tallec, G., Garnier, J., Billen, G., Gousailles, M., 2008. Nitrous oxide emissions from denitrifying
683 activated sludge of urban wastewater treatment plants, under anoxia and low oxygenation.
684 Bioresource Technology, 99(7): 2200-2209.
685 DOI:<http://dx.doi.org/10.1016/j.biortech.2007.05.025>

686 Taylor, S.W., Jaffé, P.R., 1990. Biofilm growth and the related changes in the physical properties of
687 a porous medium: 3. Dispersivity and model verification. Water Resour. Res., 26(9): 2171-
688 2180. DOI:10.1029/WR026i009p02171

689 Taylor, S.W., Milly, P.C.D., Jaffé, P.R., 1990. Biofilm growth and the related changes in the
690 physical properties of a porous medium: 2. Permeability. Water Resour. Res., 26(9): 2161-
691 2169. DOI:10.1029/WR026i009p02161

692 Toride, N., Leij, F.J., van Genuchten, M.T., 1999. The CXTFIT code for estimating transport
693 parameters from laboratory or field tracer experiments.

694 Vandevivere, P., Baveye, P., 1992. Saturated Hydraulic Conductivity Reduction Caused by Aerobic
695 Bacteria in Sand Columns. Soil Sci. Soc. Am. J.(1): 1-13.

696 Vidal-Gavilan, G., Carrey, R., Solanas, A., Soler, A., 2014. Feeding strategies for groundwater
697 enhanced biodenitrification in an alluvial aquifer: Chemical, microbial and isotope
698 assessment of a 1D flow-through experiment. Sci.Total Environ., 494–495(0): 241-251.
699 DOI:<http://dx.doi.org/10.1016/j.scitotenv.2014.06.100>

700 Wehrer, M., Jaesche, P., Totsche, K.U., 2012. Modeling the kinetics of microbial degradation of
701 deicing chemicals in porous media under flow conditions. Environ. Pollut., 168: 96-106.
702 DOI:<http://dx.doi.org/10.1016/j.envpol.2012.04.016>
703 Zheng, C., Wang, P.P., 1999. MT3DMS: A modular three-dimensional multispecies model for
704 simulation of advection, dispersion and chemical reactions of contaminants in groundwater
705 systems. Documentation and User's Guide, Contract Reo. SERDP-99-41. U.S. Army Eng.
706 Res. and Dev. Cent., Vicksburg, Miss.

707

Figure captions

Figure 1. Experimental flow-through system and location of the sampling ports.

Figure 2. Model fits using the ADE (black lines) and a dual domain model (red dashed lines). Square symbols (\square) correspond to measurements corresponding to the tracer test performed at day 0 (red and black lines run in top of each other), whereas circles (\circ) correspond to the BTC from the test at day 342. The error bars are related to the bromide analyses.

Figure 3. Results of the EIB models considering different injection strategies at the outflow of the column (70 cm). The black and the red solid lines were obtained with dispersivity values of 0.48 and 3.43 cm, respectively, considering an ADE equation. The dashed-dotted blue line corresponds to a model using a dispersivity value of 3.43 cm and a dual model mass transfer. The dashed black line corresponds to ethanol concentration in the injection solution. Grey areas represents the two periods without feeding. The bottom plot shows the simulated biomass concentrations (represented in mM) at the last cell of the model domain (70 cm).

Figure 4. Nitrate distance profiles (simulated vs. measured) at 12 different times. In each plot, the first number represents the sampling day, and that in brackets reflects the elapsed time since the last injection period. The black and the red dashed lines were obtained with dispersivity values of 0.48 and 3.43 cm, respectively, considering an ADE equation. The blue dashed dotted line in the last two plots corresponds to a model using a dispersivity value of 3.43 cm and a dual model mass transfer. The grey zone corresponds to the injection point.

Figure 5. Detail of feeding strategies with low C:N ratio without considering decay of biomass (top line) and biomass decay (bottom line). Filling zone indicates the importance of biomass decay on nitrate consumption rates under low C:N.

Figure 6. Comparison of the amount of ethanol used in injections and percentage of denitrification achieved by the different feeding strategies. The percentage of denitrification was calculated as the difference in nitrate mass between the inlet and the outlet of the column divided by the nitrate mass at the inlet.

Table captions

Table 1. Average concentration of different species in the input water. Nitrate concentration (*) varied during the experiment due to seasonal nitrate oscillations within the aquifer.

Table 2. Summary of the different feeding strategies (I to IV) tested during the experiment, in terms of feeding frequency, ethanol concentration supplied, ratio of C (external organic carbon source concentration) to N (nitrate concentration), and duration.

Table 3. Hydraulic parameters estimated for the two bromide tracer tests. The standard deviation was calculated by using the inverse problem with CTXFIT. The interpretation models were different for the two tests: the initial one (day 0) with an ADE model; the second one (day 342) with the dual domain model, thus involving two additional parameters. The R^2 of two fitted curves were 0.999 and 0.998, respectively.

749 **Table 4.** Biogeochemical constants used in the denitrification model, compared with values
750 compiled from the literature. Both the median and the standard deviation were determined
751 by automatic calibration using PEST.

752 **Table 5.** Comparison between the values obtained in this work and in similar experiments
753 compiled from the literature, including feeding strategies, organic carbon inflow, flow rate
754 and estimated increase in the dispersivity after some period of time.

Figure1
[Click here to download high resolution image](#)

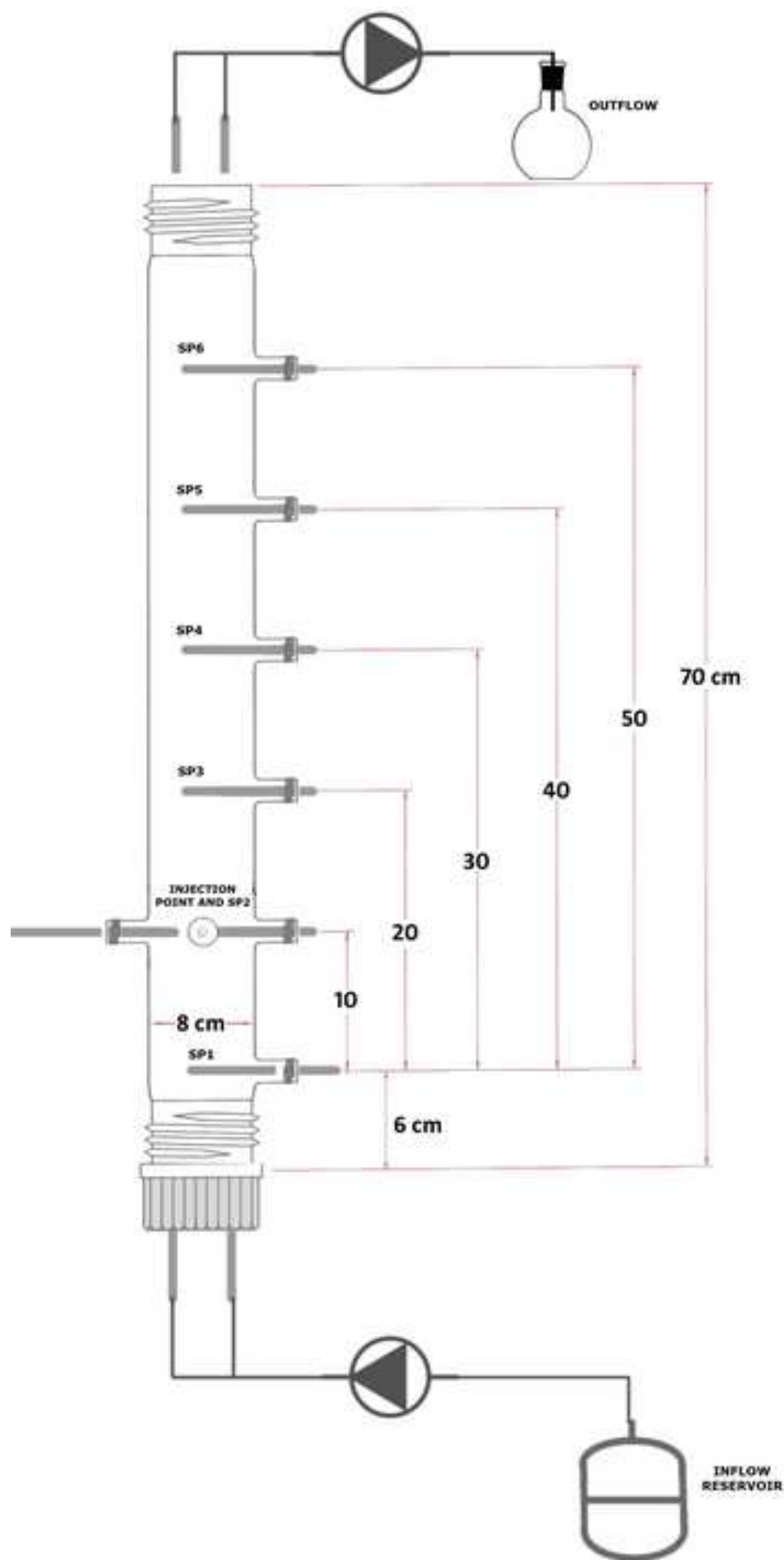


Figure2
[Click here to download high resolution image](#)

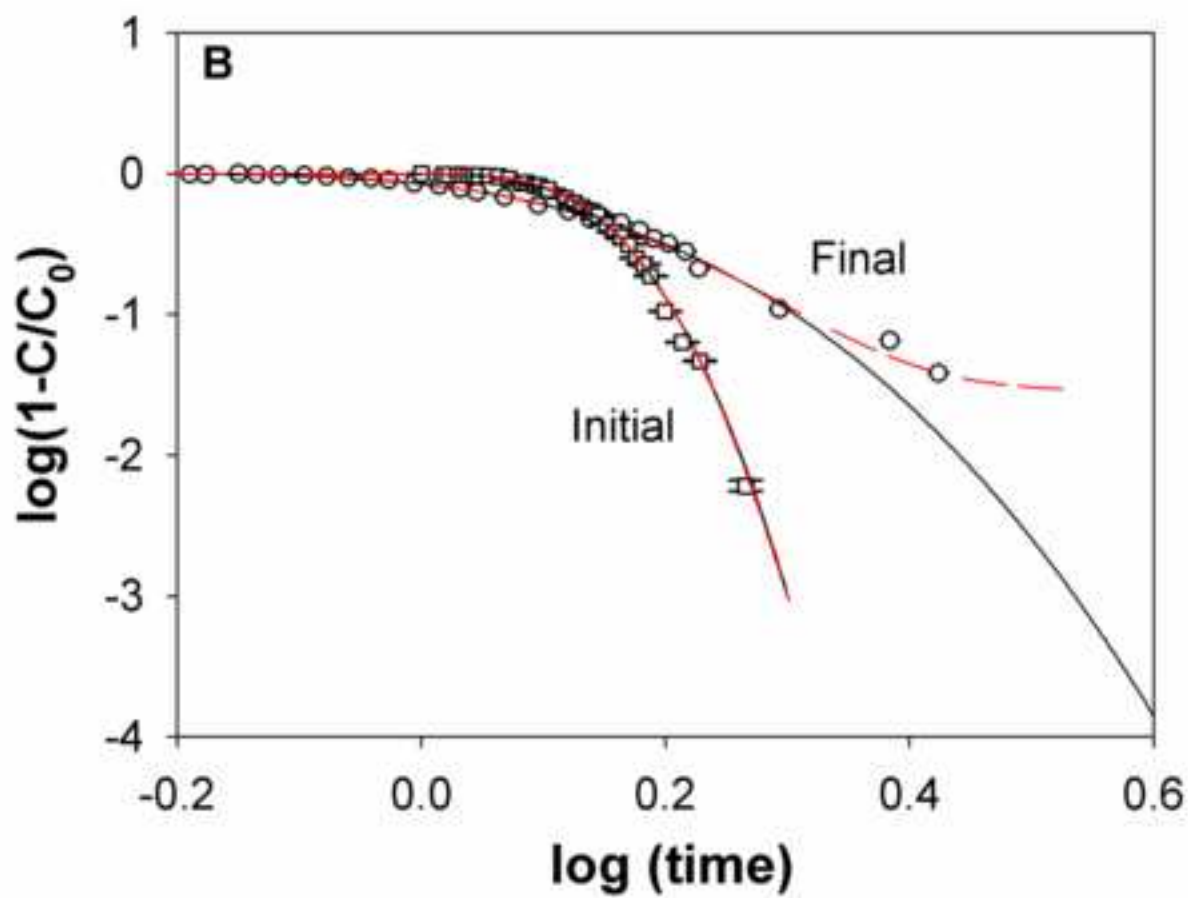
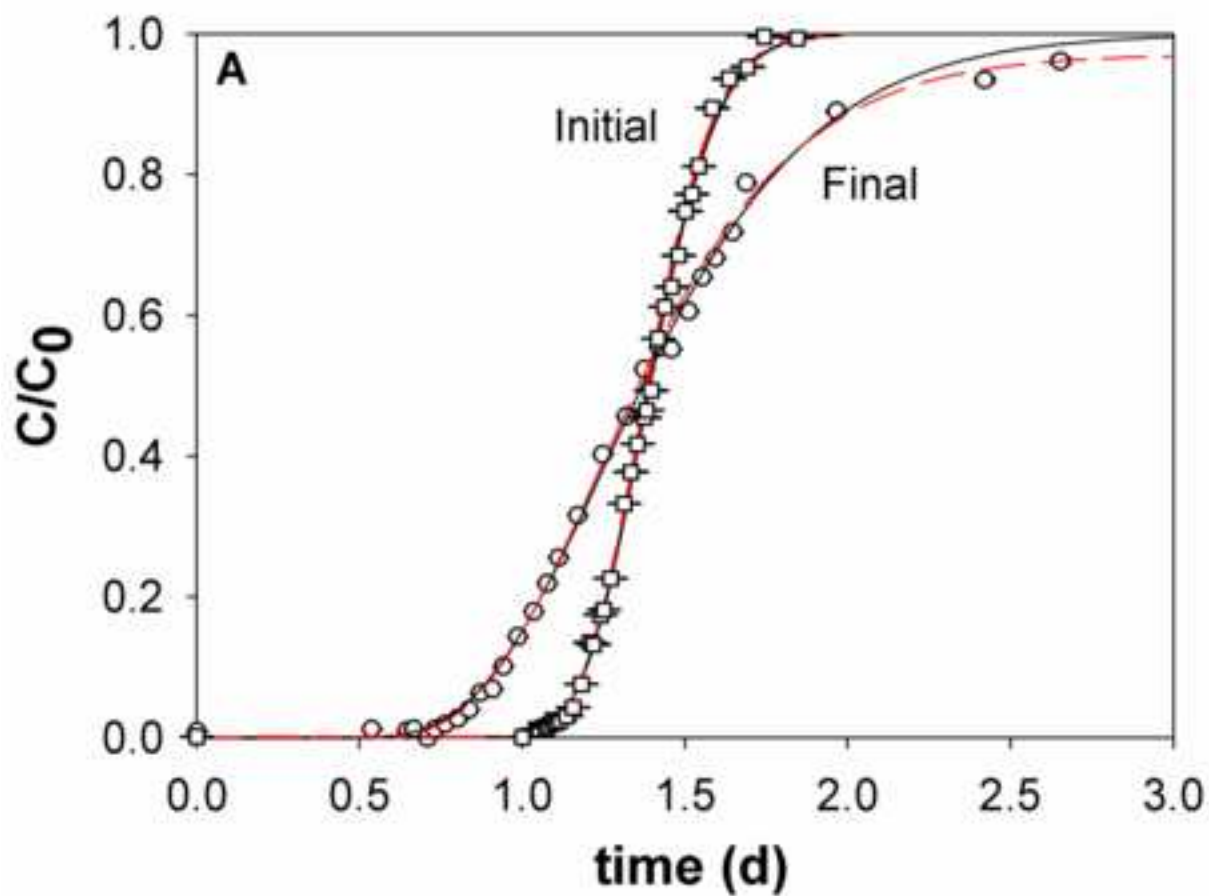


Figure3

[Click here to download high resolution image](#)

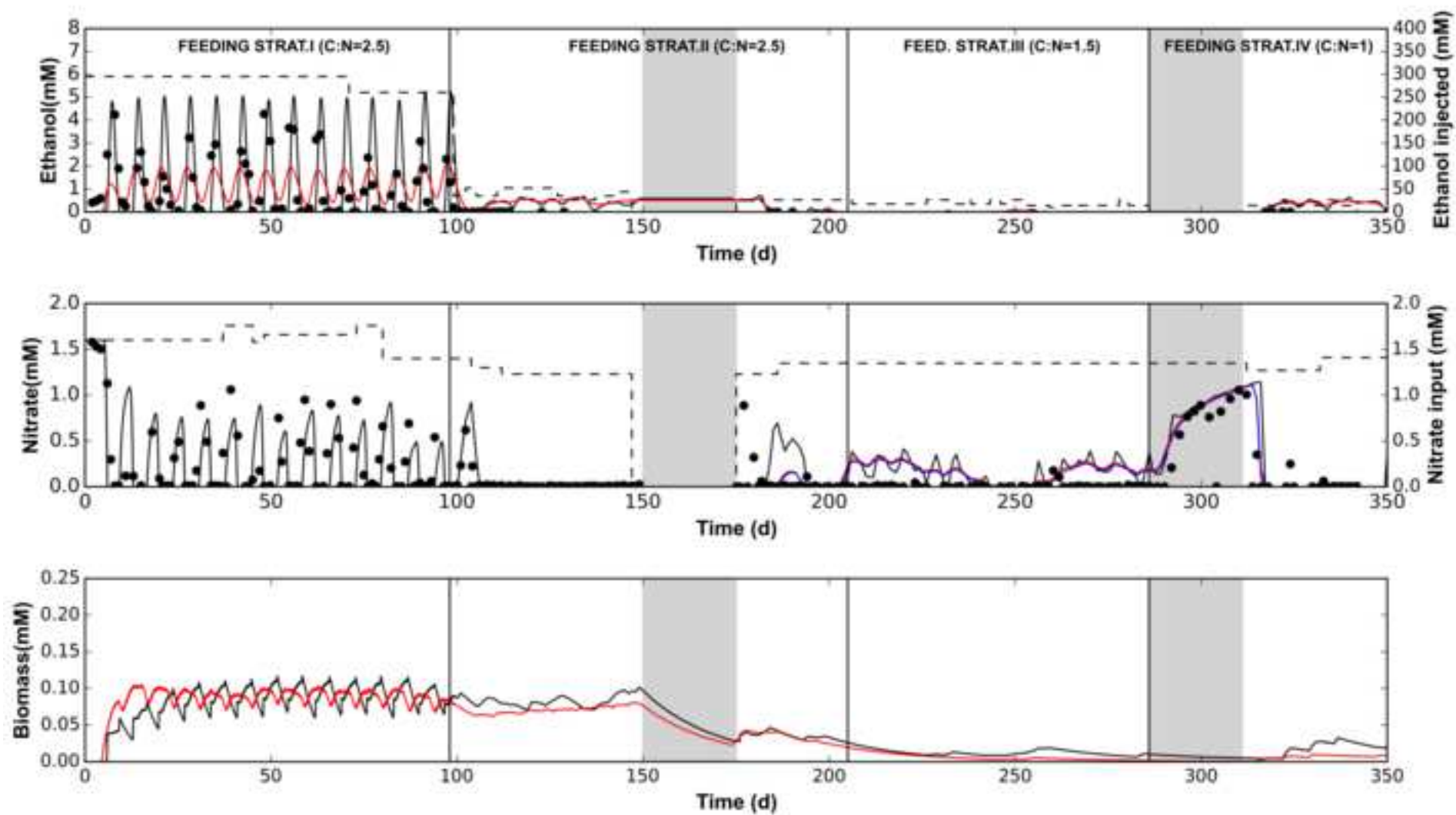


Figure4
[Click here to download high resolution image](#)

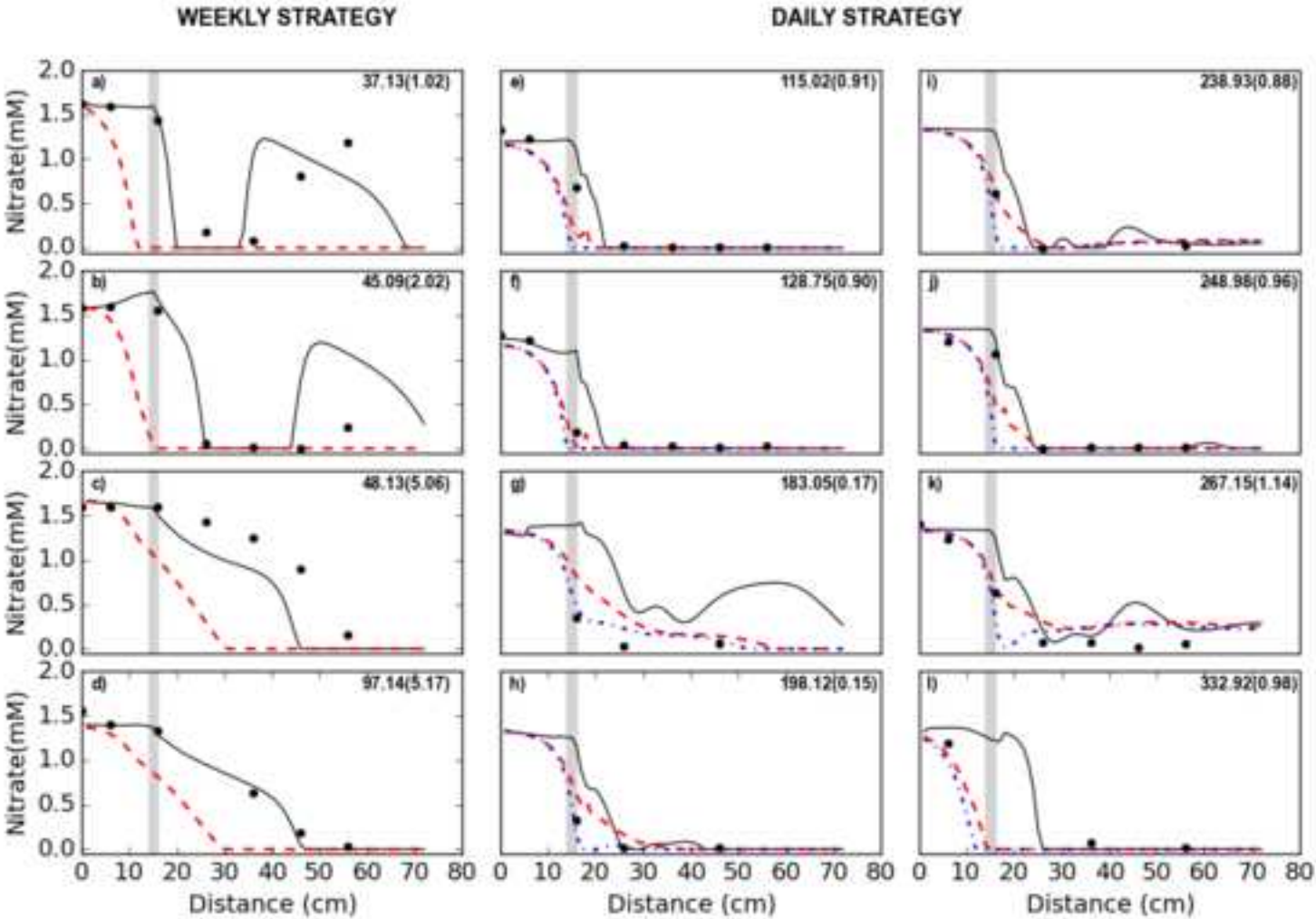


Figure5
[Click here to download high resolution image](#)

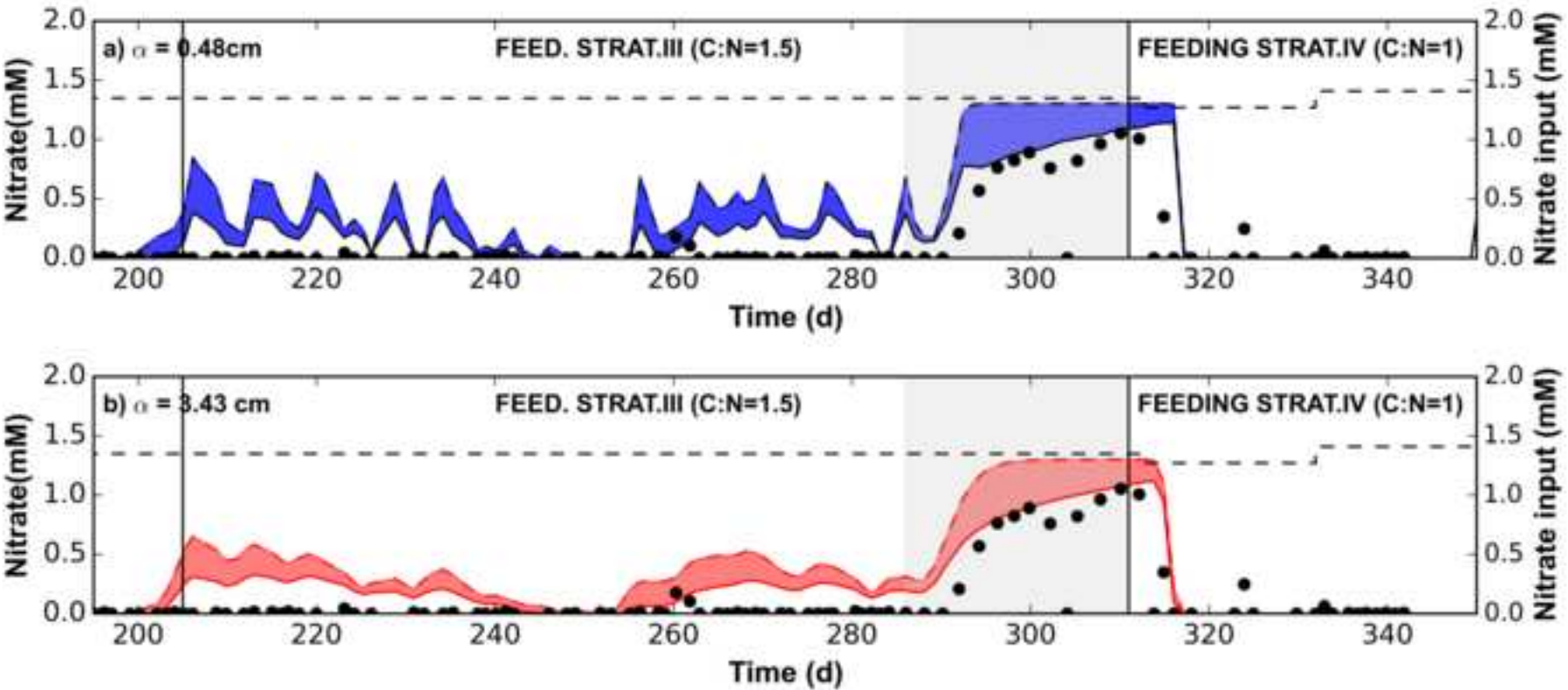


Figure6
[Click here to download high resolution image](#)

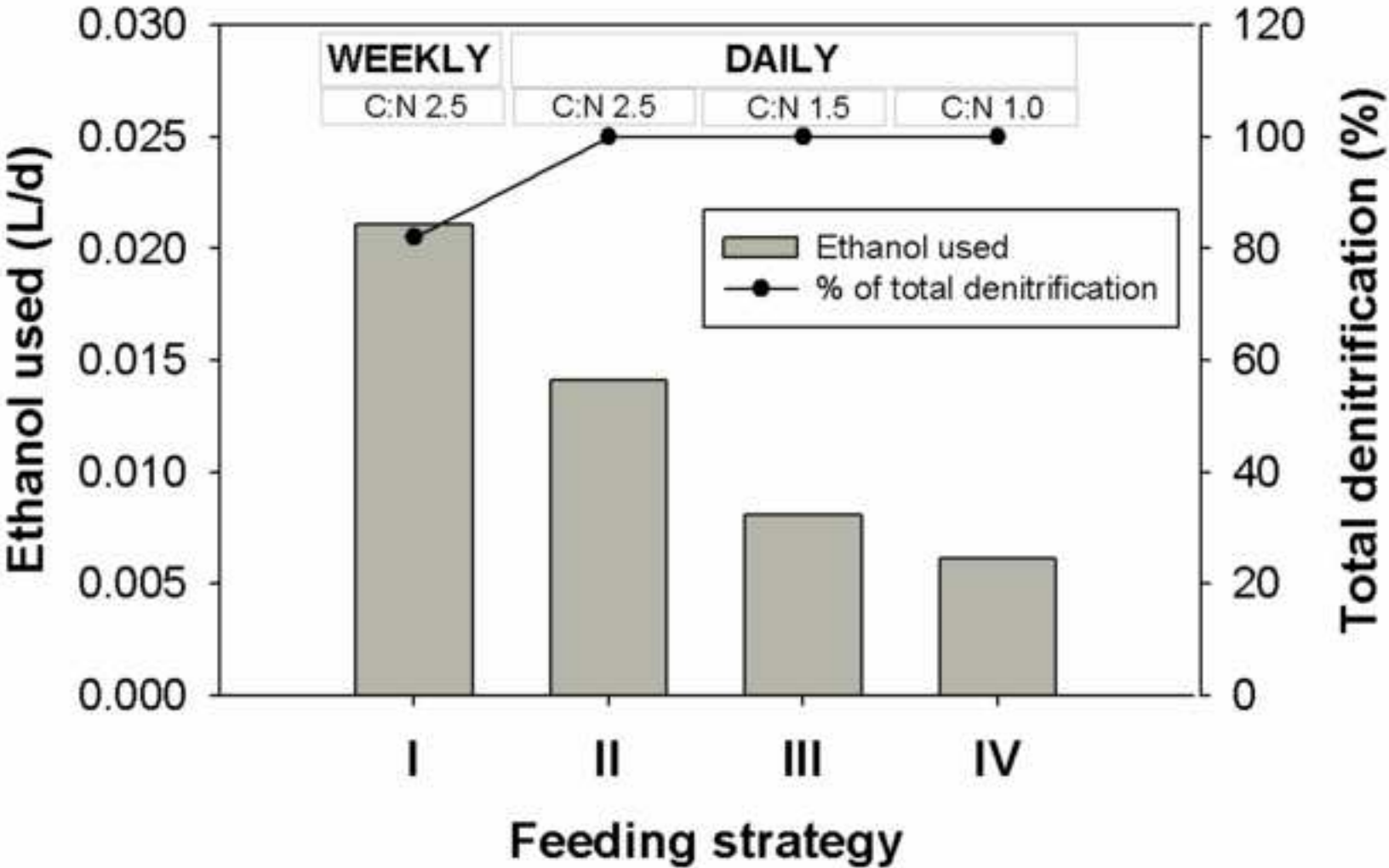


Table1
[Click here to download Table: Table1_v2.docx](#)

Parameter	Unit	Column solution	Injected solution
pH		7.2 ± 0.1	7.2 ± 0.1
Temperature	°C	15	15
Nitrate	mM	1.2-1.6 (*)	1.2-1.6 (*)
DIC	mM	7.2 ± 1.0	7.2 ± 1.0
Chloride	mM	0.10 ± 0.04	0.10 ± 0.04
Sulfate	mM	1.2 ± 0.1	1.2 ± 0.1
Calcium	mM	3.40 ± 0.07	3.40 ± 0.07
Sodium	mM	2.20 ±0.04	2.20 ±0.04
Magnesium	mM	1.60 ±0.03	1.60 ±0.03
Potassium	mM	0.100 ±0.001	0.100 ±0.001
Ethanol	mM	-	14-292
Biomass	mM	2.3 x 10 ⁻⁷	

Feeding strategy	Feeding frequency	Average C:N	Ethanol injected (mM ethanol)	Days of experiment
I	Weekly	2.5	261-292	1-98
II	Daily	2.5	26-35	99-205*
III	Daily	1.5	17	206-287
IV	Daily	1	14	287-342**

*Supply of water was discontinued between days 150 and 175

**Supply of organic carbon was discontinued between days 286 and 311

	Groundwater velocity (m d ⁻¹)	MODEL TYPE	Mobile Porosity	Dispersivity (cm)	Mass transfer parameter (α , d ⁻¹)	Immobile porosity
Initial	0.5036 ± 0.0004	ADE	0.331 ± 0.033	0.485 ± 0.006	N/A	N/A
End	0.5107 ± 0.0018	Dual domain	0.326 ± 0.044	3.440 ± 0.246	0.019± 0.018	0.015 ± 0.009

Parameter	Unit	This work	Literature values	Reference ^a
μ_{\max}	[d ⁻¹]	$3.01 \times 10^1 \pm 1.82 \times 10^1$	1×10^1 ; 1.1×10^1 ; 2×10^1 ; 1.08×10^2	1,2,3,4
$K_{S,EA}$ (nitrate)	[M]	$8.18 \times 10^{-6} \pm 4.84 \times 10^{-6}$	1.6×10^{-6} ; 3.2×10^{-6} ; 1.2×10^{-5} ; 1.8×10^{-4}	1,3,2,4
$K_{S,ED}$ (ethanol)	[M]	$1.18 \times 10^{-4} \pm 4.55 \times 10^{-5}$	8.3×10^{-6} ; 1.7×10^{-4} ; 6.6×10^{-4} ; 7.3×10^{-2}	1,2,3,4
b	[d ⁻¹]	$1.73 \times 10^{-1} \pm 4.66 \times 10^{-2}$	6×10^{-2} ; 1.5×10^{-1} ; 2×10^{-1}	2,4,3

^a References are 1, Chen and MacQuarrie (2004); 2, Lee et al., (2009); 3, Kinzelbach et al., (1991); 4, Rodríguez-Escales et al., (2014).

Table5
Click here to download Table: Table5_v2.docx

Authors	Feeding strategy	Sediment	Time of feeding strategy (d)	Biological process	Organic carbon inflow (mM C)	Velocity (m/d)	α/ α_0 (observed time)
This work	Weekly	Sand (0.5-0.8 mm)	100	Denitrification using ethanol	260-235	0.5	1 (100 d)
	Daily		200		14-35		7 (200 d)
Taylor and Jaffé (1990) and Taylor et al. (1990)	Continuous	Sand	284	Methanol oxidation (aerobic conditions)	0.22	27.2	100-1000
			356		0.17	9.1	100-1000
Bielefeldt et al. (2002)	Continuous	Sand (0.32 mm)	50	Naphthalene degradation (aerobic conditions)	1.6	3.3	1.8 (25-46)
						7.5	3-4.8 (37-44)
						11.2	2.2 (32-50)
Seifert and Engesgaard (2007)	Continuous	Sand (0.4-0.8 mm)	150	Acetate oxidation (aerobic conditions)	0.15	5.1	2 (13 d)
							7 (45 d)
Delay et al. (2013)	Continuous	Coarse crushed limestone (2 cm)	1.4	Denitrification using ethanol	1.52	34.6	1 (1.4 d)
					2.23	138.2	1 (1.4 d)